International Journal of Engineering and Management Research e-ISSN: 2250-0758 | p-ISSN: 2394-6962
Volume- 9, Issue- 2 (April 2019)
www.ijemr.net https://doi.org/10.31033/ijemr.9.2.27

An Analysis of Small Magnetic Nanoparticles Using EPR

Dr. Pawan Kumar
Associate Professor, Meerut College, Meerut, INDIA

Corresponding Author: drpkmc@gmail.com

ABSTRACT

A technique based on the gigantic spin model was used to interpret the spectra. We show the thermal development of the spin system in terms of the population of excited spin states, which confirms the quantum behaviour of MNPs. Electron magnetic resonance (EMR) spectroscopy was used to analyses magnetic nanoparticles (MNPs) of spinel type iron oxide (of approximately 4 nm) calcified inside the interior cavity of a small ferritin-type protein. EMR measurements were taken in perpendicular and parallel configurations at various temperatures.

Keywords-- EPR, Nanoparticles, Small Magnetic, Spin Model

I. INTRODUCTION

Nano magnetic systems have attracted a lot of attention in recent years as a result of its potential applications in both fundamental science and a wide range of practical industries. The advent of new properties that rely on their reduced dimensions has sparked this interest. Magnetic nanoparticles (MNPs) and molecular Nano magnets are two types of zero-dimensional magnetic objects that can be distinguished (MNMs). In general, these magnetic systems have been characterized and studied in two ways: MNPs are obtained through a top-down approach and are theoretically described by classical mechanics; MNMs, on the other hand, are obtained through a bottom-up approach and their behaviour is interpreted using quantum mechanics. The necessity for a unified picture of the two magnetic objects has recently been presented, justified by the fact that they have now achieved the same dimensions, in order to gain a better understanding of their properties. Electron magnetic resonance (EMR) investigations have provided evidence in this direction. Signatures of the discrete nature of the energy levels in MNPs have appeared in particular, demonstrating the system's quantum structure.

MNPs of spinel type iron oxide of approximately 4 nm mineralized in the interior cavity of the Dps protein were studied (a protein belonging to the ferritin family). We used the Listeria innocua (LiDps) Dps protein as a protein cage system, which differs from ferritins in its smaller size (9 nm outer and 4.5 nm inner diameters as compared to 12 and 8 nm, respectively). We were able to adjust the size and iron oxide phase of the MNPs using a previously used method [16]. In the form of magnetite/magnetite, the MNPs produced inside the protein cages contain at least 400 Fe ions.

EMR spectroscopy was used to explore the quantum behaviour of these MNPs. At various temperatures, EMR spectra were recorded in two different configurations: parallel and perpendicular, that is, with the microwave radiation's B1 field parallel and perpendicular to the external B0 field. In the two realized configurations, the possible transitions between total spin projections have different selection rules: these alternate measurements are thus a mechanism to detect and address the quantum character of the system.

We compared the EMR data to simulated MNP spectra in order to extract meaningful information. Simulations were carried out using a method based on the gigantic spin model. MNMs have used this approach to characterize the interaction of their spin ground state with the external magnetic field extensively. However, if the MNPs are thought of as an ensemble of hundreds of Fe(III) ions, each with a spin of 5/2, and a ferromagnetic coupling between them is assumed, a reasonable estimate of the overall spin of the system would be at least 1000. This would have a significant impact on the associated Hilbert space. Then we decided to take a more straightforward approach based on the notion of a system's effective lower spin, as well as spin Hamiltonian and experimental parameters. This method has previously been successful in interpreting EMR spectra in relation to MNPs calcified inside the ferritin protein.

In this paper, we demonstrate the utility of this method and use it to investigate the thermal evolution of the system's spin state in great detail. The thermal population of excited spin states causes the temperature behaviour of the spectra, we show.

II. MATERIALS AND PROCEDURES

2.1 Synthesis of MNP in LiDps Proteins

Proteins from Apo-LiDps were produced and purified as previously described. With modest adjustments, MNPs were enclosed inside the LiDps nanocage, as we had previously described. Iron incorporation studies were

e-ISSN: 2250-0758 | p-ISSN: 2394-6962
Volume- 9, Issue- 2 (April 2019)
https://doi.org/10.31033/ijemr.9.2.27

performed at 65 °C on 1 mg/mL LiDps samples in 5 mM Hepes-NaOH (Sigma Aldrich, Italy) at pH 8.5.Iron(II) sulphate heptahydrate solutions (Sigma Aldrich, Italy) dissolved in 0.5 mM HCl were used as an iron source.The reaction vessel was kept at 65 °C under positive N2 pressure throughout the experiment, and the pH was dynamically maintained at 8.5 with 100 mM NaOH using an automated titrator (TITRINO, Metrohm AG). Using two peristaltic pumps, FeSO4 (15 mM) and H2O2 (5 mM) solutions were added simultaneously and at a constant rate (0.5 mL/min). 450 Fe (II)/protein was the iron loading factor. Centrifugation at 16,000 rpm for 45 minutes at 4 °C and filtration through 0.2-m filters were used to remove any protein and iron oxide aggregates formed during MNP formation. MNPs were purified using a Superose 6 gel-filtration column equilibrated with 0.15 M HEPES-NaOH buffer at pH 7.8 and size exclusion chromatography (SEC). The protein and iron contents of MNP-containing samples were determined using native electrophoresis on 1% agarose gels and the ferrozine method, as described by Ceci et al.

2.2 EMR Spectroscopy Electromagnetic Radiation

The 9 GHz Bruker Elexys E500 apparatus (Bruker, Rheinstetten, Germany) with a microwave frequency counter was used to do X-band EMR measurements. The low temperatures were achieved with an Oxford Instruments ESR 900 continuous He flow cryostat. EPR spectra were obtained using a microwave power of 26 W in the perpendicular configuration and 21 mW in the parallel configuration, with a field modulation of 100 kHz and 5 G. The measurements were made with a Bruker ER-4116DM EPR-resonator (Rheinstetten, Germany).

III. THEORETICAL FRAMEWORK

Simulations were run for both configurations at each temperature to understand the EMR spectra observed for MNPs growing inside LiDps proteins. The massive spin associated with the entire MNP was used in these simulations. Based on previously published data [16], the saturation magnetization (measured at 1.8 K) and the anisotropy field Ba were found to be 59.7 emu g1 and 0.3 T, respectively. The magnetic moment of each MNP may be calculated using the formula = MSVp, where MS is the volume magnetization and Vp is the particle volume; for MNPs inside LiDps, MS is equivalent to 298.5 emu cm3 (based on a density of 5 g cm3 for magnetite or magnetite) and the particle radius is 1.7 nm.

The relationship can be established using these facts this facilitates the evaluation of the current state. a spin value on the order of 300; moreover, a D value of around-13 MHz (4.3 10^{-4} cm^{-1}) is discovered.

Given these estimated S and D values, the enormous size of the Hilbert space associated with the system prompted us to use a simplified simulation approach, employing a smaller effective spin value and, as a result, a smaller effective spin Hamiltonian and experimental parameters, as we had previously done successfully on MNPs mineralized in the interior of the ferritin protein [19]. In a nutshell, this approach is predicated on the ability to recreate the EMR spectrum of spin S MNPs using an effective lower spin value (where n is an integer and the value is positive). As a result of this assumption, it is necessary to also define a successful strategy D value D_{eff} = nd and an appropriate temperature based on the spin system's D value and the experimental temperature T, respectively. After that, the spin Hamiltonian employed in this system is

$$H = \mu_B \hat{S}_{\text{eff}} \cdot g \cdot \vec{B} + \hat{S}_{\text{eff}} \cdot \hat{D}_{\text{eff}} \cdot \hat{S}_{\text{eff}} \qquad (1)$$

The Zeeman term is the first term, while the zero fields splitting term is the second. An effective spin of 10 (i.e. n = 30) has been used to imitate the EMR spectra of MNPs in LiDps, corresponding to a spin value of 300. The use of a similar D_{eff} ~-400 MHz, on the other hand, did not allow for satisfactory simulations of the experimental spectra over the entire temperature range and for both configurations. Instead, two different effective spin states and, as a result, two different effective D values were used (D_1 *and* D_2). To recreate the experimental spectra, the corresponding simulated spectra were blended at each temperature using two separate temperature dependent weights (α(T) and (βT)). As a result, the simulated spectrum at temperature T is as follows:

$$Spec(T) = \alpha(T) Spec1(S_1, D_1, T) + \beta(T) Spec2(S_2, D_2, T) \qquad (2)$$

Spec1 (S_1, D_1, T) and Spec2 (S_2, D_2, T) are the spectra simulated at a fixed T with the D values D_1 and D_2 associated with the spin states S1 and S_2, respectively. With this method, we account for the effect of excited spin states in the EPR spectra, as these are expected to be extremely close to the ground spin state. The best

e-ISSN: 2250-0758 | p-ISSN: 2394-6962
Volume- 9, Issue- 2 (April 2019)
https://doi.org/10.31033/ijemr.9.2.27

simulations were obtained by employing two spin states with S_{eff} = 10 and an identical n value of 30 (one with a D value of 500 MHz and the other with a D value of 200 MHz) for each configuration at each temperature. As a result, each experimental spectrum was modeled as the result of contributions from two equal spin states (S = 300) with two different D values. We employed two distinct strains on the D values (i.e., two different widths for the D distributions) in conjunction with D1 and D2; these values are the same for every temperature and setup. $Dstrain_1$ = 50 MHz and $Dstrain_2$ = 200 MHz (only in the perpendicular case at 5 K, it was necessary to use a $Dstrain_1$ of 500 MHz and to also introduce a strain on E of 100 MHz). Furthermore, the line widths associated with the resonance of the two states have been modified for each temperature and configuration. Easy spin was used to simulate the spectra.

Figures 3 and 4 shows the comparison of the experimental and simulated spectra at each temperature for both setups (the same images, including the contributions due to S_1 and S_2, are reported in the Supplementary Info). In the perpendicular instance, the agreement between the actual data and the simulation is excellent at 150 K: the simulation depicts the resonance at B_0 as well as a lower-intensity resonance at $B_0/2$. Until 30 K, this pattern is well reflected, but in the low field area, there is an increasing disparity between the observations and the simulations. At 15 K and 5 K, the agreement is lower, but the simulations still work.

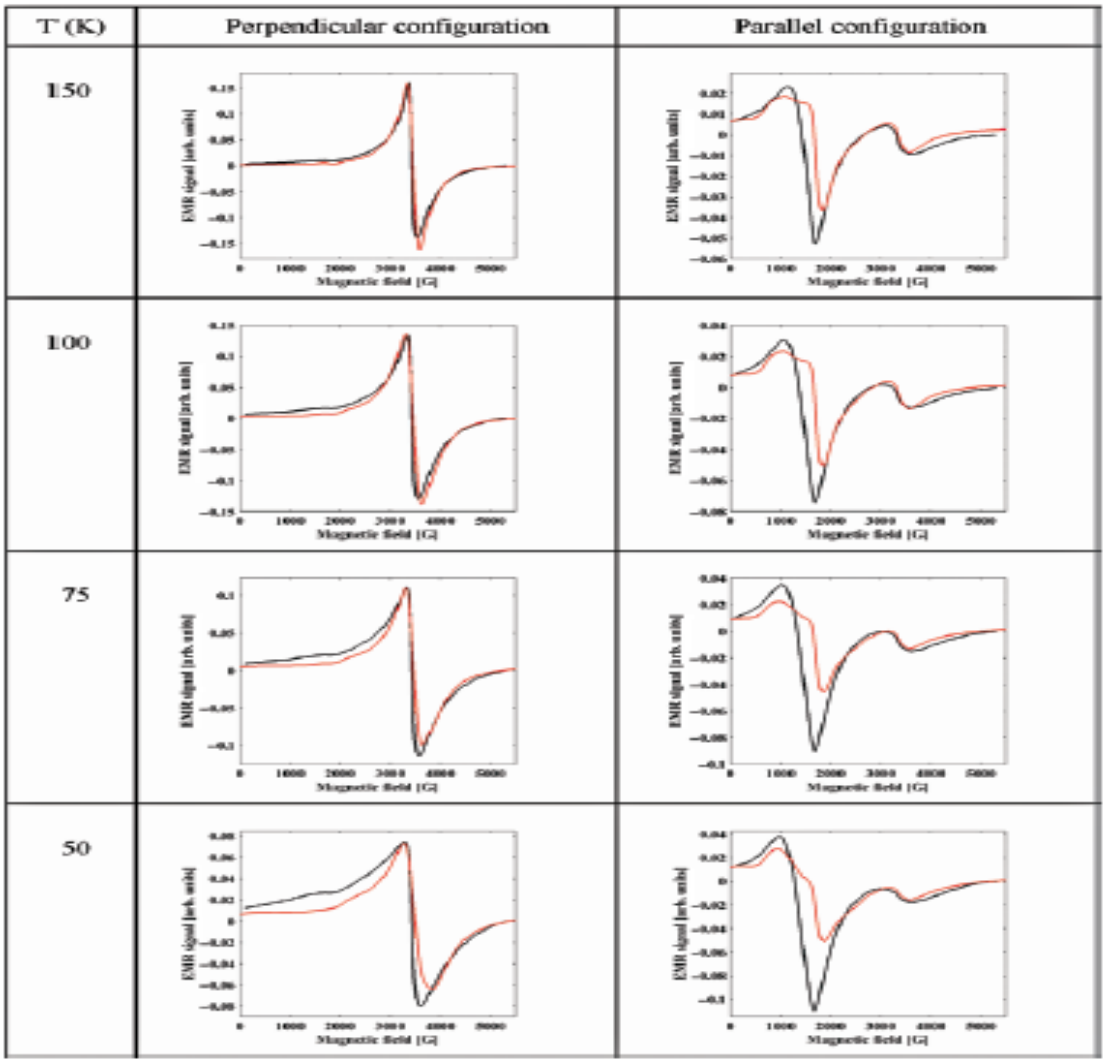

Fig. 3: Experimental EMR spectra (black line) acquired in the parallel and perpendicular configurations at 150 K, 100 K, 75 K and 50 K and corresponding simulations (red line). The simulated spectrum is the result of the combination between two systems with S_{eff} = 10 and different *D* values and linewidths.

e-ISSN: 2250-0758 | p-ISSN: 2394-6962
Volume- 9, Issue- 2 (April 2019)
https://doi.org/10.31033/ijemr.9.2.27

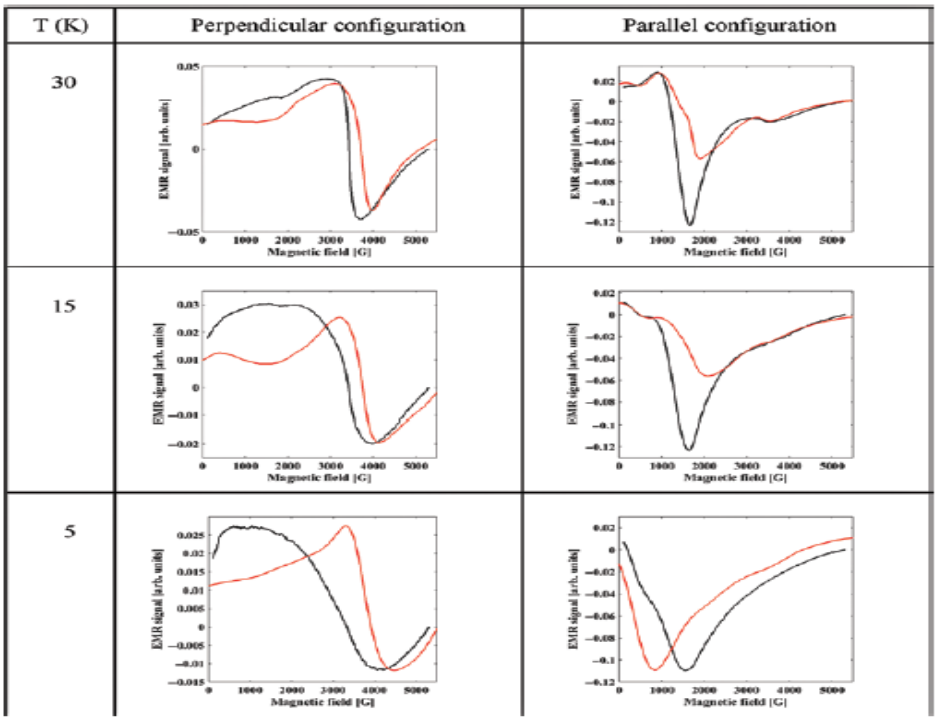

Fig. 4: Experimental EMR spectra (black line) acquired in the parallel and perpendicular configurations at 30 K, 15 K and 5 K and corresponding simulations (red line). The simulated spectrum is the result of the combination between two systems with $S_{eff} = 10$ and different D values and linewidths.

Provide the correct trend in a high field. In the parallel configuration, the situation is fairly similar: at 150 K, the agreement is good, though there is a little shift between the experimental spectrum and the simulation. At low fields, there is an increasing loss of intensity in the simulated data between 75 K and 15 K, although the agreement is still adequate. At 5 K, however, the measured spectrum is well reproduced.

The temperature dependence of the α(T) and β(T) parameters, which were used to integrate the two spectra corresponding to the two S states (with two distinct temperatures), is shown in Figure 5.

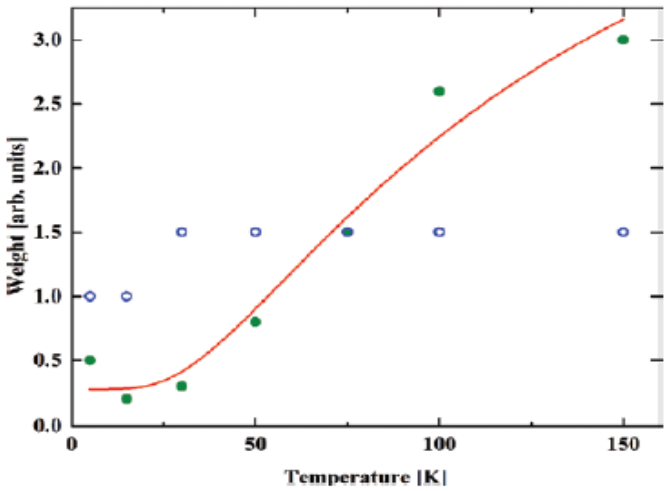

Fig. 5: Temperature dependence of the $\alpha(T)$ (blue circles) and $\beta(T)$ (green dots) parameters used to combine the simulated spectra relative to the S_1 and S_2 states. The red line is a fit of the $\beta(T)$ parameter by means of an exponential function.

e-ISSN: 2250-0758 | p-ISSN: 2394-6962
Volume- 9, Issue- 2 (April 2019)
https://doi.org/10.31033/ijemr.9.2.27

The values (D values) are reported. At each temperature, the same values were taken into account for both perpendicular and parallel experimental configurations. While α(T) (the weight corresponding to the state with D_1 = 500 MHz) remains $\beta(T) = a + be^{\left(-\frac{T_0}{T}\right)}$nt with temperature, β(T) (the weight corresponding to D_2 = 200 MHz) declines. Analyzing the thermal evolution of the α(T) and β(T) parameters is enlightening. We used an exponential fit to fit this behavior the form's function (Figure 5 depicts the fit.) The fit parameters are as follows: a = 0.3 0.2, b = 6.2 1.3, and T0 = (115 26) K.

The temperature dependency of the line widths used to simulate the spectra for the two contributions for both configurations is shown in Figure 6. These values vary between the two states and configurations, but they all follow the same temperature trend: they rise as the temperature falls. Furthermore, whereas line widths corresponding to S1 show minimal change below 50 K, line widths related to S2 show a significant increase.

The temperature behaviour of the double integral of the EMR spectra acquired in both experimental settings, as well as those derived from simulations, is shown in Figure 7. Although both setups essentially reproduce the pattern, the agreement is better at higher temperatures. The spectra's broad character, especially at low temperatures, renders it useless

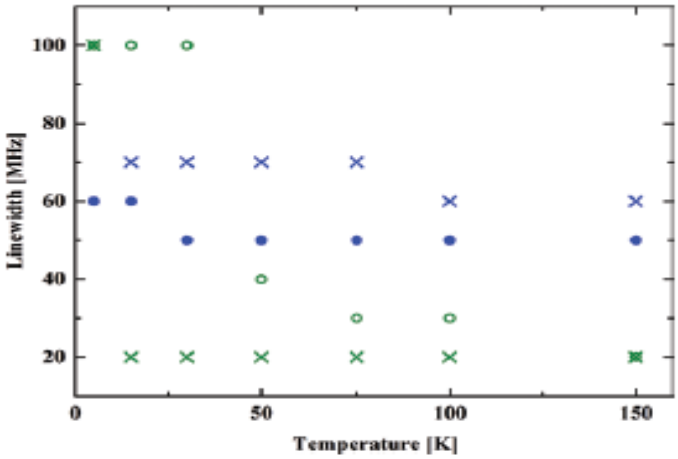

Fig. 6: Temperature dependence of the linewidths used for the spectra relative to S_1 (in blue) and S_2 (in green) in the perpendicular and the parallel configuration (dots and crosses, respectively).

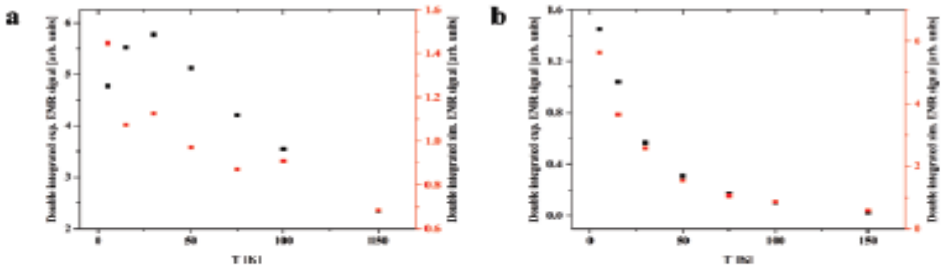

Fig. 7: Temperature dependence of the double integral of the experimental EMR spectra (black) acquired in both experimental configurations, perpendicular (a) and parallel (b), and of the simulated EMR spectra (red).

the assessment of the double integral is more difficult. Furthermore, at low temperatures, the difference between the experimental and model spectra is greater. The blocking temperature in relation to the experimental technique [27] has been attributed to the maximum found in the experimental data of Figure 7a.

IV. RESULTS

At temperatures ranging from 150 K to 5 K, EMR spectra of MNPs internalized inside LiDps proteins were obtained in both perpendicular and parallel configurations at X-band. Figures 1 and 2 show the results of these measurements, respectively. A resonance at a field B_0 of

e-ISSN: 2250-0758 | p-ISSN: 2394-6962
Volume- 9, Issue- 2 (April 2019)
https://doi.org/10.31033/ijemr.9.2.27

roughly 3400 G is visible in the spectrum recorded at 150 K in the perpendicular configuration.

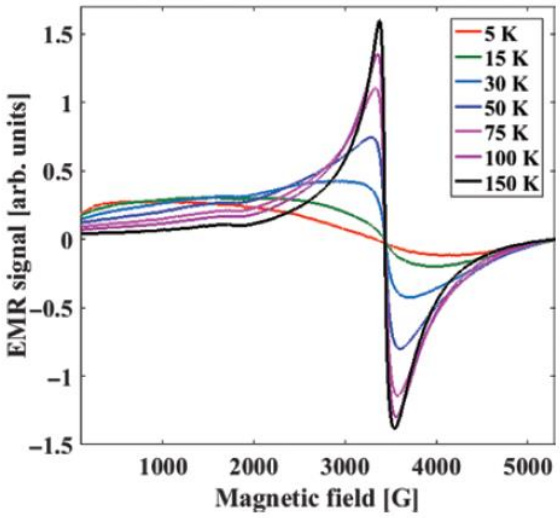

Fig. 1: EMR spectra of MNPs in LiDps proteins acquired at X-band in perpendicular configuration at various temperatures. The microwave frequency used was 9.64 GHz.

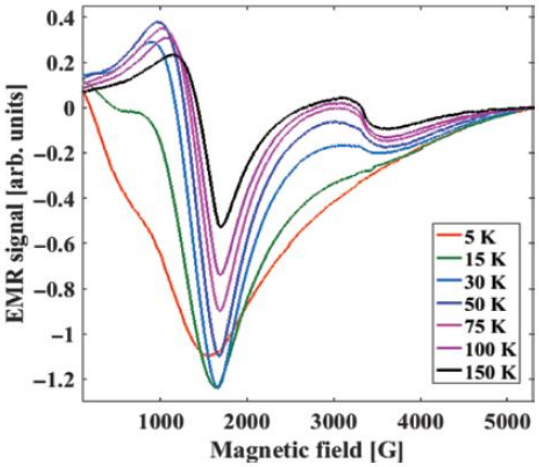

Fig. 2: EMR spectra of MNPs in LiDps proteins acquired at X-band in parallel configuration at various temperatures. The microwave frequency used was 9.40 GHz.

When the temperature is lowered, the resonance becomes broader and shifts to a lower value. At higher temperatures, there is also the presence of a band with a low intensity at a field around half B0.This band is due to "partially" forbidden transitions between spin states with $\Delta M = \pm 2$, where M is the expectation value of S_z and S is the MNP's total spin. The spectra recorded in the parallel configuration support this interpretation. At $B_0/2$, Figure 2 shows an effective increase in the signal from the MNPs. Finally, as in the perpendicular case, as the temperature is reduced, the spectra become broader and shift to a minor field value.

V. DISCUSSION & CONCLUSION

In order to better understand the thermal history of the system's spin states, we ran comprehensive simulations for all of the observed temperatures and in both experimental configurations, assuming a random orientation of the MNPs' easy axes in the frozen suspension. We found that simulating the MNP system as a combination of two subsystems with the same effective spin but differing D values was necessary (and so was a different corresponding strain over them). Because the combination of the two spin states resulted in temperature dependence, this rules out the idea that it describes sample

heterogeneity. The spectra acquired for the perpendicular and parallel configurations may be simulated using an identical combination of these two subsystems. We wish to underline that using the same parameters to reproduce data from two distinct experimental settings is a test for the parameters' confidence, keeping in mind that the system is significantly more intricate, and the approach used provides a simplified and fair depiction of its behaviour. Combining two separate subsystems provides a method of accounting for the thermal population of spin states in MNPs. As MNMs teach us, as the number of magnetic centers increases, the excited spin states become closer in energy to the fundamental spin state, therefore they must be taken into account in the thermal evolution of the EMR spectra (see and references therein). Other terms in the spin Hamiltonian, while viable, are of secondary importance in our opinion when it comes to the inclusion of excited spin states for two reasons. To begin, we should recollect that the separation between the first excited spin state and the ground spin state for the MNM Fe_{19} is 8 K, and that this is projected to decrease as the number of magnetic centers increases, e.g. for Fe_8, it is 24 K (see and references therein). Second, an axial anisotropy for the resonance position of the main resonance is derived from the angular dependence of EMR spectra acquired in a perpendicular orientation for a solution of MNPs frozen in an external magnetic field, with no indication of higher order contributions to the spin Hamiltonian.

For temperatures ranging from 150 K to 5 K, EMR spectra of MNPs calcified inside the LiDps protein were obtained in perpendicular and parallel configurations. A simplified version of the gigantic spin model was used to interpret the spectra. The main feature of this reduced approach is the replacement of the large spin value associated with the system with a smaller effective spin value; in this case, we used an effective spin value of 10 for each MNP inside the LiDps protein instead of an estimated spin value of 300. We used the same approach with the inclusion of a temperature-dependent parameter, exemplifying a non-isotropic distribution of easy axes in our previous work on MNPs mineralized in the ferritin protein; the spectra were then simulated after a discretization over the angle between the easy axis of the ZFS tensor and the direction of the external magnetic field. The fact that the spin state defining the system does not remain constant with temperature prompted the establishment of that temperature-dependent component.

EMR measurements in the X-band are presented in this paper. The Zeeman interaction is of the same order of magnitude as the ZFS interaction in this band: as the external field value is increased, the ratio between the transitions at $B_0/2$ and B_0 is expected to decrease dramatically, as has already been demonstrated by comparing X-band and W-band measurements [16], emphasizing the quantum nature of the system.

The temperature T_0, which is determined by fitting the β(T) value, indicates the energy separation between the energy levels of the spin states under consideration. The value we get from the fit is a little higher than predicted. However, we believe that this figure is influenced by the worse quality of our simulations at low temperatures; the difference between measured and simulated spectra in this thermal range may lead to an overestimation.

To summarize, we have shown that a modified version of the giant spin model can be used to efficiently simulate EPR spectra of MNPs; with the proposed approximation, we can simulate EMR spectra of huge S values while describing the system with the same spin Hamiltonian parameters in both configurations for a wide range of temperatures. Finally, this description enables the quantum behavior of MNPs to be demonstrated.

REFERENCES

[1] D. Gatteschi, M. Fittipaldi, C. Sangregorio, & L. Sorace, Angew. (2012). *Chemie Int*. Ed. 51.
[2] M. Alex C. Innocenti, P. Ceci, C. Sangregorio, L. Castelli, L. Sorace, & D. Gatteschi. (2011). Phys. rev. B condens. matter mater. *Phys. 83*, 104409.
[3] Innocenti, C. Sangregorio. (2015). Chem. *A Eur. J., 16*, 709.
[4] N. Noginova, T. Weaver, E. P. Giannelis, A. B. Bourlinos, V. A. Atsarkin, & V. V. Demidov. (2011). Phys. Rev. B – Condens. matter mater. *Phys. 77*.
[5] K. Fittipaldi, R. Mercatelli, S. Sottini, P. Ceci, E. Falvo, & D. Gatteschi. (2016). Phys. Chem. Chem. *Phys. 18*, 3591.
[6] A.-L. Barra, L.-C. Brunel, D. Gatteschi, L. Pardi, & R. Sessoli. (2007). *Acc. Chem. Res. 31*, 460.
[7] D. Gatteschi, A. L. Barra, A. Caneschi, A. Cornia, R. Sessoli, & L. Sorace, Coord. (2015). Chem. Rev.250, 1514.
[8] E. J. L. McInnes. (2010). Spectroscopy of single-molecule magnets. Germany: Springer.
[9] R. S. Edwards, S. Maccagnano, E. C. Yang, S. Hill, W. Wernsdorfer, D. Hendrickson, & G. Christou. (2013). *J. Appl. Phys. 93*, 7807.